J Math Chem (2015) 53:911–924
DOI 10.1007/s10910-014-0448-4

ORIGINAL PAPER

DRBEM solution of natural convective heat transfer with a non-Darcy model in a porous medium

B. Pekmen · M. Tezer-Sezgin

Received: 10 July 2014 / Accepted: 27 November 2014 / Published online: 6 December 2014

Abstract This study presents the dual reciprocity boundary element (DRBEM) solution of Brinkman–Forchheimer-extended Darcy model in a porous medium containing an incompressible, viscous fluid. The governing dimensionless equations are solved in terms of stream function, vorticity and temperature. The problem geometry is a unit square cavity with either partially heated top and bottom walls or hot steps at the middle of these walls. DRBEM provides one to obtain the expected behavior of the flow in considerably small computational cost due to the discretization of only the boundary, and to compute the space derivatives in convective terms as well as unknown vorticity boundary conditions using coordinate matrix constructed by radial basis functions. The Backward-Euler time integration scheme is utilized for the time derivatives. The decrease in Darcy number suppresses heat transfer while heat transfer increases for larger values of porosity, and the natural convection is pronounced with the increase in Rayleigh number.

Keywords DRBEM · Natural convection · Porous medium · Brinkman–Forchheimer-extended Darcy model

Mathematics Subject Classification 76S99 · 76R10 · 76D05 · 65M38

B. Pekmen (✉)
Department of Mathematics, Atilim University, Ankara, Turkey
e-mail: bengisenpekmen@gmail.com

M. Tezer-Sezgin
Department of Mathematics and Institute of Applied Mathematics,
Middle East Technical University, Ankara, Turkey
e-mail: munt@metu.edu.tr

1 Introduction

Natural convective heat transfer in a porous medium has taken the great deal of interest in recent years due to its importance in many engineering applications such as packed bed reactors, drying processes, electronic cooling, geothermal energy systems, thermal insulation.

A chemical reaction between a foreign mass (e.g. porous surface) and the fluid occurs in many chemical engineering processes. The diffusion and chemical reaction cause buoyancy effects resulting with heat and mass transfer in porous media. These processes in a porous medium have industrial applications such as the polymer production, food processing and synthesis of ceramic materials.

There are lots of studies considering different models of porous medium fluid flows. Theoretical and applied explanation details can be found in the books [14,15].

In the literature, most of the numerical studies are concentrated on the flow models for porous medium such as Brinkman-extended Darcy and/or Brinkman–Forchheimer-extended Darcy model (which is also mentioned as non-Darcy flow model). Brinkman viscous terms are included in both models, but only the quadratic inertial terms are added in the latter model. The importance of inertial terms is having a stabilization influence on the fluid flow and heat transfer due to the increase in inertial terms corresponding to the decrease in Darcy number.

On Brinkman-extended Darcy model (BDM), Das et al. [5] focused, and used the finite element method (FEM) with isoparametric, quadrilateral elements for stability. Using an iterative finite difference scheme (FDM) with uniform node distribution, Pakdee et al. [19] also studied the same model. Jecl et al. [6] investigated modified BDM for natural convection flow in a porous square cavity saturated with a non-Newtonian fluid utilizing the boundary element method (BEM).

The Brinkman–Forchheimer-extended Darcy model (BFDM) is studied both experimentally and numerically by Beckermann et al. [2] in which control-volume method with SIMPLER algorithm is used. Nithiarasu et al. [16] solved BFDM with a semi-implicit time scheme with Galerkin's weighted residual method and a pressure-velocity correction procedure. In this study, 41×41 nonuniform grids are used, and BDM is also studied analyzing the variable porosity. Utilizing the Galerkin's finite element method (FEM) with a correction algorithm, Nithiarasu et al. [17] also investigated the effect of porosity on natural convective flow and heat transfer based on BFDM model. Bhuvaneswari et al. [3] examined the influence of aspect ratio on the flow and heat transfer in a differentially heated porous enclosure modeled by BFDM employing finite volume method (FVM) with SIMPLE and a projection algorithm to handle pressure. With the same method on a specified grid distribution, Chen et al. [4] presented BFDM in a wavy porous enclosure. Also, in a two-sided lid-driven porous cavity, mixed convection flow for BFDM is investigated using multigrid approach based on FVM with SIMPLE algorithm in [11]. In a rotating, differentially heated porous enclosure, Saleh et al. [22] considered the BFDM applying the finite difference schemes both in time and space. They figured out the effect of rotational speed on heat transfer. Lam et al. [12] analyzed the heat transfer and entropy generation in a fluid-saturated porous medium with two heat sources on top and bottom walls using the streamline upwind Petrov-Galerkin based FEM and 101×101 grids. Karimi-Fard

et al. [7] and Al-Farhany et al. [1] have solved the double-diffusive natural convection in a porous medium in the same model utilizing finite volume method with SIMPLE and a projection algorithm to handle pressure.

Sarler et al. [23] solved Darcy-Brinkman model by DRBEM using the augmented scaled thin plate splines in different shape function boundary elements analyzing the various node distributions. Khashan et al. [10] investigated the thermal non-equilibrium model taking into account the Forchheimer terms utilizing FVM with SIMPLEX algorithm to handle the pressure equation. Li et al. [13] concentrated on a channel with staggered porous blocks modelled by Brinkman–Forchheimer equations. They considered the thermal conductivity ratio between the porous blocks as well as porous block height using the FVM with SIMPLER algorithm. In different forms of the porous models, Khanafer et al. [9] observed the behavior of the flow in a wavy enclosure using FEM in nine node quadrilateral elements with bi-quadratic interpolation functions. In a similar problem geometry, Kumar et al. [21] also presented the Forchheimer-extended Darcy model for a wide range of physical parameters with FEM.

In this paper, the DRBEM is used to solve Brinkman–Forchheimer-extended Darcy model in a porous medium in terms of stream function, vorticity and temperature iteratively. The boundary-only nature of DRBEM provides one to obtain the results at a small computational expense. To the authors' knowledge, this model is not solved in stream function, vorticity and temperature variables by using DRBEM.

2 Mathematical model equations

The two-dimensional, unsteady, laminar flow of a Newtonian, incompressible, viscous fluid is considered. Viscous dissipation is neglected. The physical properties of the fluid are constant except the density variation following from Boussinesq approximation. The porous medium is homogeneous and isotropic. Also, the fluid, and the solid matrix are in local thermal equilibrium. The governing equations in terms of the velocity $\mathbf{u} = (u, v)$, pressure p and temperature T are written as [18]

$$\nabla.\mathbf{u} = 0 \tag{1a}$$

$$\frac{\mu_e}{\rho}\nabla^2\mathbf{u} = \frac{1}{\epsilon_p}\frac{\partial \mathbf{u}}{\partial t} + \frac{1}{\epsilon_p^2}\mathbf{u}.\nabla\mathbf{u} + \frac{1}{\rho}\nabla p + \frac{\mu}{\rho\kappa}\mathbf{u} + \frac{c_F}{\sqrt{\kappa}}|\mathbf{u}|\mathbf{u} + \mathbf{g}\beta(T - T_c) \tag{1b}$$

$$\alpha_e\nabla^2 T = \sigma\frac{\partial T}{\partial t} + \mathbf{u}.\nabla T \tag{1c}$$

where μ_e is the viscosity in Brinkman model, μ is the dynamic viscosity of the fluid, ρ is the density of the fluid, ϵ_p is the porosity of the porous medium, κ is the permeability of the porous medium, $|\mathbf{u}| = \sqrt{u^2 + v^2}$, $\mathbf{g}$ is the gravitational acceleration vector, β is the thermal expansion coefficient, T_c is the cold wall temperature, $\alpha_e = k_e/(\rho c_p)_f$ is the effective thermal diffusivity with the effective thermal conductivity $k_e = \epsilon_p k_f +$

$(1-\epsilon_p)k_s$ of the porous medium and specific heat c_p, and [14]

$$c_F = \frac{1.75(1-\epsilon_p)}{d_p\,\epsilon_p^3} \quad \text{and} \quad \kappa = \frac{d_p^2\,\epsilon_p^3}{150(1-\epsilon_p)^2}, \tag{2}$$

are the form coefficient and the permeability of the porous medium, respectively, with the solid particle size d_p in a porous medium. Notice that the heat capacity ratio $\sigma = \dfrac{\epsilon_p(\rho c_p)_f + (1-\epsilon_p)(\rho c_p)_s}{(\rho c_p)_f}$ is taken as 1 as well as the same thermal conductivity is taken for the fluid and solid matrix ($k_e = k_f = k_s$ is taken, so is $k_e = k_f = k_s$ and $\alpha_e = \alpha_f = \alpha$) in which subscripts f and s refer to fluid and solid, respectively. Also, $\mu_e = \mu$ is considered accordance with the experimental data [2,6].

In order to make Eq. 1 dimensionless, the non-dimensional parameters are defined as

$$x' = \frac{x}{L}, \quad y' = \frac{y}{L}, \quad u' = \frac{uL}{\alpha}, \quad v' = \frac{vL}{\alpha}, \tag{3}$$

$$p' = \frac{pL^2}{\rho\alpha^2}, \quad t' = \frac{t\alpha}{L^2}, \quad T' = \frac{T-T_c}{T_h-T_c}, \tag{4}$$

where L is the characteristic length, T_h is the temperature of the hot wall. Substituting these variables in Eq. 1, and then dropping the prime notation, we obtain

$$\nabla.\mathbf{u} = 0 \tag{5a}$$

$$\frac{Pr}{\epsilon_p}\nabla^2 u = \frac{1}{\epsilon_p}\frac{\partial u}{\partial t} + \frac{1}{\epsilon_p^2}\left(u\frac{\partial u}{\partial x} + v\frac{\partial u}{\partial y}\right) + \frac{\partial p}{\partial x} + \frac{Pr}{Da}u + \frac{C_f}{\sqrt{Da}}|\mathbf{u}|u \tag{5b}$$

$$\frac{Pr}{\epsilon_p}\nabla^2 v = \frac{1}{\epsilon_p}\frac{\partial v}{\partial t} + \frac{1}{\epsilon_p^2}\left(u\frac{\partial v}{\partial x} + v\frac{\partial v}{\partial y}\right) + \frac{\partial p}{\partial y} + \frac{Pr}{Da}v + \frac{C_f}{\sqrt{Da}}|\mathbf{u}|v - Ra\,Pr\,T \tag{5c}$$

$$\nabla^2 T = \frac{\partial T}{\partial t} + u\frac{\partial T}{\partial x} + v\frac{\partial T}{\partial y}. \tag{5d}$$

where $C_f = \dfrac{1.75}{\sqrt{150}\,\epsilon_p^{1.5}}$.

The definitions of velocity components in terms of stream function are $u = \partial\psi/\partial y$, $v = -\partial\psi/\partial x$ satisfying the continuity condition. Using these in the definition of vorticity $w = \nabla \times \mathbf{u}$ gives the stream function equation. The cross-differentiation and subtraction of Eqs. (5c) and (5b) give the vorticity transport equation. Thus, the dimensionless governing equations in terms of stream function, temperature T and vorticity w ($w = \partial v/\partial x - \partial u/\partial y$) are deduced as

$$\nabla^2\psi = -w \tag{6a}$$

$$\nabla^2 T = \frac{\partial T}{\partial t} + u\frac{\partial T}{\partial x} + v\frac{\partial T}{\partial y} \tag{6b}$$

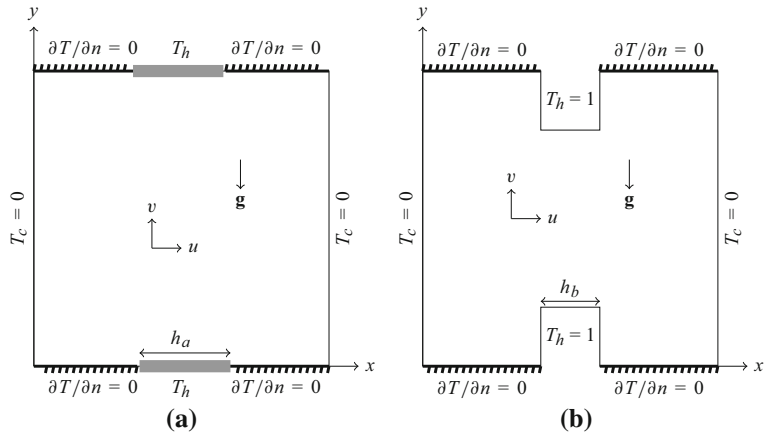

Fig. 1 Problem configuration. **a** Heated parts on top and bottom. **b** Heated steps on top and bottom

$$\nabla^2 w = \frac{1}{Pr}\frac{\partial w}{\partial t} + \frac{1}{\epsilon_p Pr}\left(u\frac{\partial w}{\partial x} + v\frac{\partial w}{\partial y}\right) + \frac{\epsilon_p}{Da}w + \frac{C_f \epsilon_p}{\sqrt{Da}\,Pr}\left(v\frac{\partial |\mathbf{u}|}{\partial x} - u\frac{\partial |\mathbf{u}|}{\partial y} + |\mathbf{u}|w\right) - \epsilon_p Ra\frac{\partial T}{\partial x}, \tag{6c}$$

and the non-dimensional parameters Darcy number Da, Rayleigh number Ra and Prandtl number Pr are [14]

$$Da = \frac{\kappa}{L^2},\ Ra = \frac{g\beta\Delta T L^3}{\nu\alpha},\ Pr = \frac{\nu}{\alpha}. \tag{7}$$

Here, $\nu = \mu/\rho$ is the kinematic viscosity and $\Delta T = T_h - T_c$.

The problem geometries are depicted in Fig. 1. Two heated ($T_h = 1$) parts and square hot obstacles are placed on the top and bottom walls. Jagged walls are adiabatic while the left and right walls are cold walls $T_c = 0$. No-slip boundary conditions are imposed on each wall ($u = v = \psi = 0$).

3 DRBEM solution

DRBEM is a boundary only discretization method, and gives the solution directly on the boundary, and at some required interior points. DRBEM treats all the terms other than Laplacian as inhomogeneity in the equations, and thus, the fundamental solution of Laplace equation is made use of as the case of BEM solutions of Poisson's equation. The resulting system matrices of equations are generally small in size compared to all other domain discretization methods. This provides a computationally cheap procedure. Also, DRBEM has the advantage of computing all the space derivatives in the equations and unknown vorticity boundary values by using DRBEM coordinate matrix.

The terms on the right hand side of Eq. (6) are treated as inhomogeneous terms in the application of DRBEM, and are approximated by [20]

$$b_i \approx \sum_{j=1}^{N_I+N_B} \alpha_j f_{ij}, \tag{8}$$

where N_I is the number of arbitrarily located interior points, N_B is the number of boundary points, α_j's are sets of initially unknown coefficients, and the f_{ij}'s are approximating functions in a relation with particular solution $\nabla^2 \hat{u}_{ij} = f_{ij}$. f_{ij}'s are radial basis functions (RBFs) which depend on the radial distance $r_{ij} = \sqrt{(x_i - x_j)^2 + (y_i - y_j)^2}$ in which i and j are the indices indicating source (fixed) and the field (variable) points, respectively. Radial basis functions may be chosen as polynomials, splines, Gaussian, or multiquadrics.

Multiplication of both sides of differential Eqs. (6a)–(6c) ($\nabla^2\varphi = \sum_{j=1}^{N_I+N_B} \alpha_j \nabla^2 \hat{u}_{ij}$, where φ stands for ψ, T or w) by the the fundamental solution of Laplace equation ($u^* = -\ln(r)/(2\pi)$), and integration over the domain gives the integrals over the domain Ω as

$$\int_\Omega (\nabla^2\varphi) u^* d\Omega = \sum_{j=1}^{N_B+N_I} \alpha_j \int_\Omega (\nabla^2 \hat{u}_j) u^* d\Omega. \tag{9}$$

Then, the key point of DRBEM is to use the Divergence theorem for the Laplacian term on both sides of equation providing one to obtain all integrals on the boundary as

$$c_i\varphi_i + \int_\Gamma \varphi \frac{\partial u^*}{\partial n} d\Gamma - \int_\Gamma \frac{\partial \varphi}{\partial n} u^* d\Gamma = \sum_{j=1}^{N_B+N_I} \alpha_j \left(c_i \hat{u}_{ij} + \int_\Gamma \hat{u}_j \frac{\partial u^*}{\partial n} d\Gamma - \int_\Gamma \frac{\partial \hat{u}_j}{\partial n} u^* d\Gamma \right),$$

where $c_i = 0.5$ if the boundary Γ is a straight line and $i \in \Gamma$, and $c_i = 1$ when node i is inside.

The boundary is discretized by N_B linear elements. The boundary integrals are evaluated over each element by a numerical quadrature, and then an assembly procedure for all elements is achieved. Thus, Eqs. (6) may be written in a matrix-vector form as

$$\mathbf{H}\varphi - \mathbf{G}\varphi_q = (\mathbf{H}\hat{\mathbf{U}} - \mathbf{G}\hat{\mathbf{Q}})\mathbf{F}^{-1} b, \tag{10}$$

where the entries of the matrices $\mathbf{H}$ and $\mathbf{G}$ contain the boundary integrals of the fundamental solution u^*, and the normal derivative of u^*, respectively, $\mathbf{F}$ is the coordinate matrix constructed from the RBFs f_{ij}'s, $\hat{\mathbf{U}}$ and $\hat{\mathbf{Q}}$ matrices have the entries computed by the particular solution $\hat{u}_{ij}$ and its normal derivative $\hat{q}_{ij} = \partial \hat{u}_{ij}/\partial n$. The coordinate matrix $\mathbf{F}$ is also used to compute the space derivatives in inhomogeneous terms, e.g.

$$\frac{\partial \varphi}{\partial x} = \frac{\partial \mathbf{F}}{\partial x}\mathbf{F}^{-1}\varphi, \quad \frac{\partial \varphi}{\partial y} = \frac{\partial \mathbf{F}}{\partial x}\mathbf{F}^{-1}\varphi. \tag{11}$$

Utilizing the DRBEM with Backward-Euler finite difference in the time derivatives, the matrix-vector form of Eqs.(6) is obtained as

$$\mathbf{H}\psi^{m+1} - \mathbf{G}\psi_q^{m+1} = -\mathbf{S}w^m \tag{12a}$$

$$\left(\mathbf{H} - \frac{1}{\Delta t}\mathbf{S} - \mathbf{SM}\right) T^{m+1} - \mathbf{G}T_q^{m+1} = -\frac{1}{\Delta t}\mathbf{S}T^m \tag{12b}$$

$$\begin{aligned}\left(\mathbf{H} - \frac{1}{Pr\,\Delta t}\mathbf{S} - \frac{1}{\epsilon_p Pr}\mathbf{SM} - \frac{1}{\epsilon_p Da}\mathbf{S}\right) w^{m+1} &= -\frac{1}{Pr\,\Delta t}\mathbf{S}w^m \\ &\quad + \frac{c_f \epsilon_p}{\sqrt{Da}\,Pr}\mathbf{S}\left(K + |\mathbf{u}|_d^{m+1} w^m\right) \\ &\quad - \mathbf{S}\epsilon_p Ra \mathbf{D_x} T^{m+1},\end{aligned} \tag{12c}$$

where $\mathbf{S} = (\mathbf{H}\hat{\mathbf{U}} - \mathbf{G}\hat{\mathbf{Q}})\mathbf{F}^{-1}$, $\mathbf{D_x} = (\partial\mathbf{F}/\partial x)\mathbf{F}^{-1}$, $\mathbf{D_y} = (\partial\mathbf{F}/\partial y)\mathbf{F}^{-1}$, $\mathbf{M} = u^{m+1}\mathbf{D_x} + v^{m+1}\mathbf{D_y}$, $u^{m+1} = \mathbf{D_y}\psi^{m+1}$, $v^{m+1} = -\mathbf{D_x}\psi^{m+1}$, $|\mathbf{u}|^{m+1} = \sqrt{(u^2)^{m+1} + (v^2)^{m+1}}$, $K = ([v]_d^{m+1}\mathbf{D_x} - [u]_d^{m+1}\mathbf{D_y})|\mathbf{u}|^{m+1}$, with the subscript d corresponding to diagonal, and m is the iteration level.

The unknown vorticity boundary conditions are also computed with the help of coordinate matrix $\mathbf{F}$, i.e.

$$w = \nabla \times \mathbf{u} = \frac{\partial v}{\partial x} - \frac{\partial u}{\partial y} = \mathbf{D_x}v - \mathbf{D_y}u, \tag{13}$$

which is used at each time iteration m.

The system of Eqs. (12a)–(12c) are rearranged with the insertion of the known and unknown boundary information, and the reduced form of the systems $\mathbf{A}x = b$ are solved by Gaussian elimination with partial pivoting at each time iteration. At initial time, w^0 and T^0 are taken as zero everywhere except on the boundary. Once the stream function is found, the velocity components, and thus the magnitude of the velocity, are computed, and then their boundary values are inserted. The velocity components u and v are made use of in the energy and vorticity equations, respectively. The iteration continues until the criterion [8]

$$\frac{\left\|\psi^{m+1} - \psi^m\right\|_\infty}{\left\|\psi^{m+1}\right\|_\infty} + \frac{\left\|T^{m+1} - T^m\right\|_\infty}{\left\|T^{m+1}\right\|_\infty} + \frac{\left\|w^{m+1} - w^m\right\|_\infty}{\left\|w^{m+1}\right\|_\infty} < \epsilon \tag{14}$$

is satisfied with a tolerance $\epsilon = 10^{-5}$.

Average Nusselt number through the top and bottom heated walls is computed, respectively, by

$$\overline{Nu}_t = \int_{\text{top}} \frac{\partial T}{\partial n} ds, \qquad \overline{Nu}_b = \int_{\text{bottom}} \frac{\partial T}{\partial n} ds, \tag{15}$$

where $\partial T/\partial n$ is the normal derivative of T, and $ds = dx$ or $ds = dy$.

Table 1 Validation case with $\epsilon = 0.4,\ Pr = 1$

Da	Ra	c	N, L	$\overline{Nu}$	[16]
10^{-2}	10^3	0.001	80,625	1.00	1.01
	10^4	0.02	80,625	1.405	1.408
	10^5	0.065	80,625	2.987	2.983
10^{-4}	10^5	0.007	80,441*	1.065	1.067
	10^6	0.0077	80,441*	2.55	2.55
	10^7	0.0054	80,441*	7.81	7.81
10^{-6}	10^7	0.0037	88,529*	1.078	1.079
	10^8	0.0037	88,529*	2.99	2.97
	10^9	0.0025	88,529*	11.45	11.46

Table 2 Grid analysis with respect to $\overline{Nu}_t$ keeping $Ra = 10^5,\ c = 0.0035$

Case 1 ($N_I = 729$)			Case 2 ($N_I = 815$)		
N_B	$Da = 10^{-2}$	$Da = 10^{-3}$	N_B	$Da = 10^{-2}$	$Da = 10^{-3}$
80	3.8240	3.1616	96	3.1314	2.4906
104	3.8783	3.2545	144	3.1764	2.5767
128	3.9112	3.3170	192	3.2023	2.6226
152	3.9362	3.3635	240	3.2137	2.6507

4 Numerical results

In the computations, multiquadric radial basis function $f = \sqrt{c^2 + r^2}$ with shape parameter c, and 8-point Gaussian quadrature is used in the construction of **H** and **G** matrices. Prandtl number is fixed as $Pr = 0.71$. Natural convection flow behavior is visualized in terms of streamlines, isotherms, and vorticity contours for various Da and Ra. In some cases, once the vorticity is obtained, a relaxation parameter is used as $w^{m+1} \leftarrow \gamma w^{m+1} + (1-\gamma)w^m$ for accelerating the convergence in which $0 < \gamma < 1$. Although there are some studies optimizing the value of c, we determine the value of c (in the flow behavior) by trial and error in terms of convergence.

As a validation case, the proposed numerical scheme is also applied to the problem defined in [16], and the average Nusselt number values through the hot wall is compared in Table 1. In this table, $\Delta t = 0.1 = \gamma$ is used in all cases, and the grid distribution for the results with $Da = 10^{-2}$ is uniform boundary nodes with Gauss-Chebyshev-Lobatto (GCL) interior points while the results denoted by '*' are obtained by GCL nodes on both boundary and interior. Uniform node distribution with small number of boundary and interior points gives also satisfying results for reasonable values of Ra, but the number of nodes should be increased for large values of Ra. Therefore, we used the non-uniform grid distribution in this Table, and these type of nodes endure oscillations at large Ra, and gives better results than uniform nodes. As is seen, our results are in good agreement with the results in reference [16] at a small computational expense.

In the following both problems, the uniform grid distribution on the boundary and the GCL nodes in the interior are adopted. A grid analysis is also given in Table 2

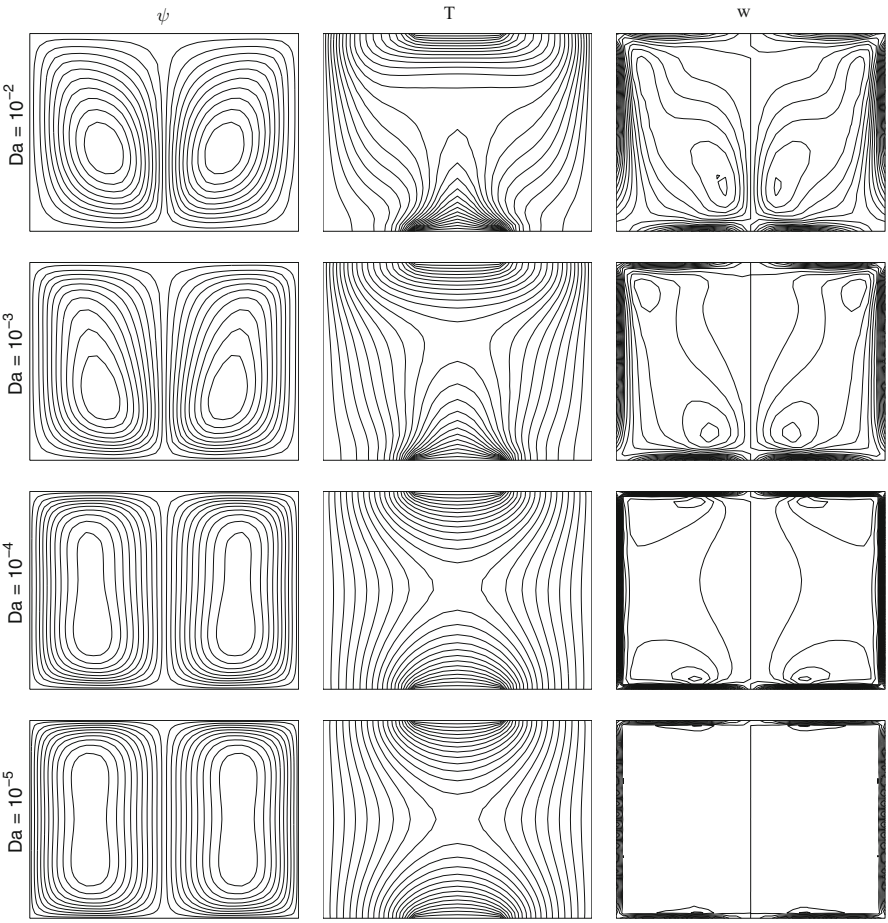

Fig. 2 $Ra = 10^5, \epsilon_p = 0.6, c = 0.0035$

showing the dependence of average Nusselt numbers on the number of boundary elements through the heated top walls of the cavities. Regarding this table, in general, $N_B = 128$ linear boundary elements with $N_I = 729$ interior grid points in Case 1, and $N_B = 144$ linear boundary elements with $N_I = 815$ interior nodes in Case 2 are used. Larger values of Ra require more boundary elements and interior nodes. Furthermore, the number of boundary elements and interior nodes also change as the size of the heaters are altered.

4.1 Case 1: Partially heated top and bottom walls

In this case, h_a is taken as $1/3$ (Fig. 2) and $1/7$ (Fig. 3).

In Fig. 2, the center of two symmetric, counter-rotating cells of streamlines in the direction of gravity expands, and form boundary layers through the top and bottom

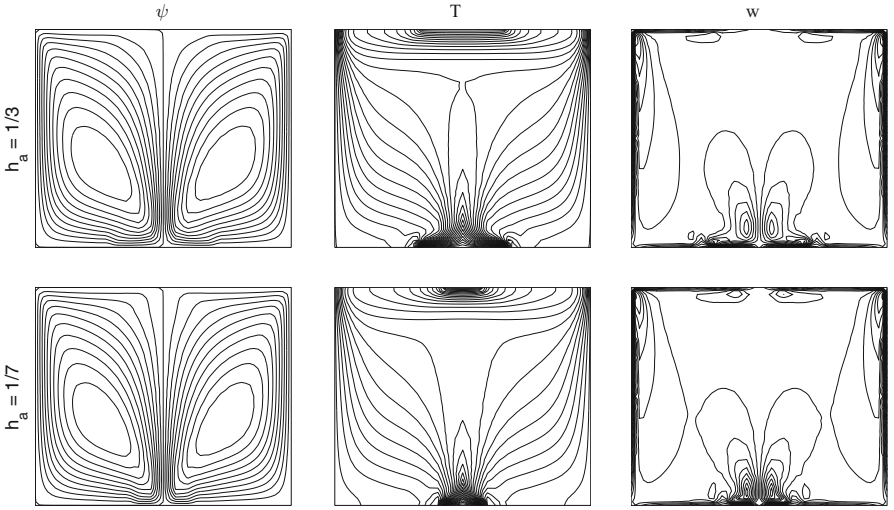

Fig. 3 The change in the size of the partial wall on *top* and *bottom* with $\epsilon_p = 0.6,\ Ra = 10^7,\ Da = 10^{-4},\ \gamma = 0.5,\ c = 0.0055,\ \max|\psi| = 13.8,\ \max|\psi| = 11.9,\ N_B = 248,\ N_I = 961$

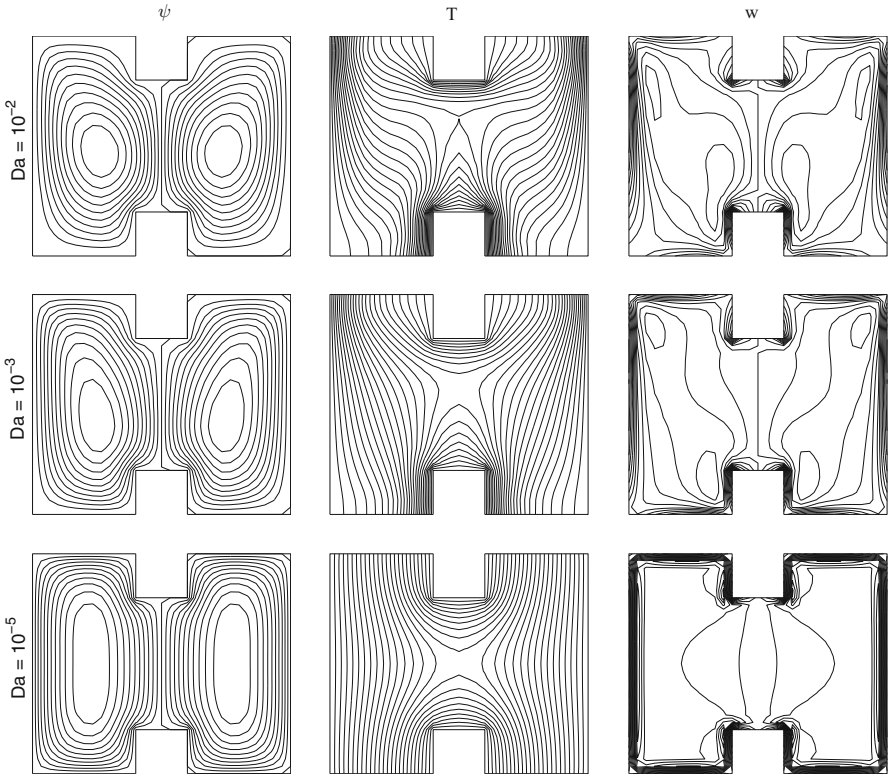

Fig. 4 Darcy variation $Pr = 0.71,\ Ra = 10^5,\ \epsilon_p = 0.6,\ \Delta t = 0.1,\ c = 0.003$

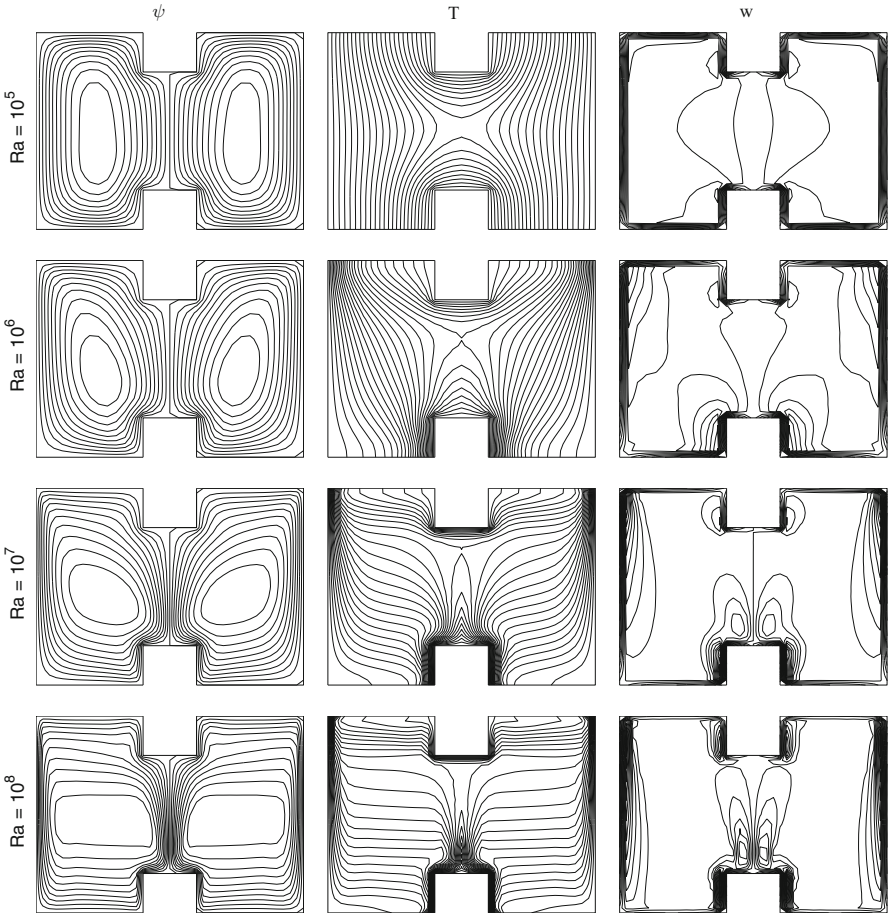

Fig. 5 Rayleigh variation $Da = 1e-4$, $Pr = 0.71$, $\epsilon_p = 0.6$, $\Delta t = 0.1$, $N = 144$, $K = 815(Ra = 10^5, 10^6(\gamma = 1.0))$, $N = 192$, $K = 1455(Ra = 10^7(\gamma = 0.4), 10^8, \gamma = 0.05)$

walls as Da decreases. This points to the decrease in the flow circulation. In other words, the fluid flows slowly. Isotherms becomes nearly perpendicular to adiabatic walls, and symmetrically intensified around the heated parts at small Da numbers while the heat rises up (convection) from bottom heated wall to top one at large Da values. Vorticity almost becomes stagnant at the center as Da decreases.

With an increase in Ra when $Da = 10^{-4}$, $h_a = 1/3$ (Fig. 3), fluid circulation increases, and the boundary layer formation for streamlines between symmetric cells is pronounced. The center of streamlines takes a sharp form in the direction of gravity. Isotherms exhibit a natural convective behavior for large values of Ra due to the dominance of buoyancy effect. Vorticity also verifies the intensity of convection with the emerge of two symmetric circulations on bottom heated wall. In Fig. 3, the change in the size $h_a = 1/7$ of the heated wall is also observed. Not much variation is seen on flow behavior, but a little bit fluid velocity, and thus the natural convection, decreases since the heated parts are decreased.

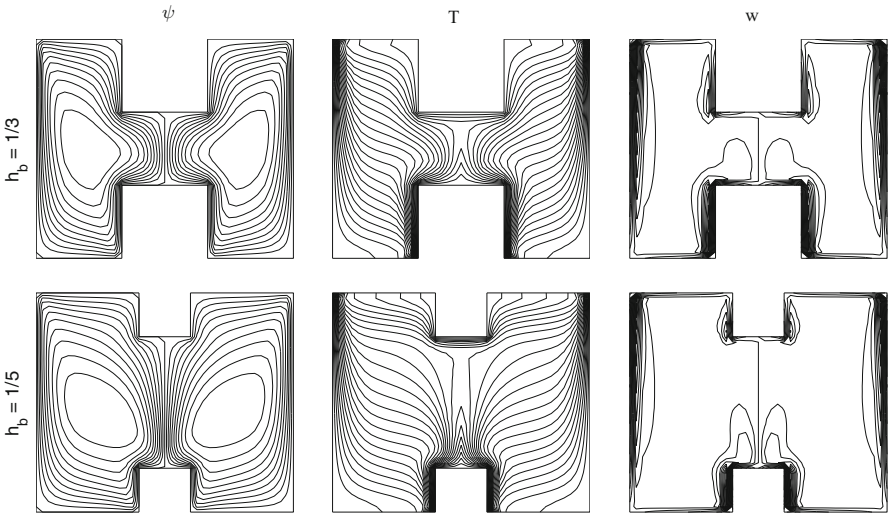

Fig. 6 $Da = 10^{-5}$, $Ra = 10^8$, $c = 0.003$, $\gamma = 0.5, \overline{Nu}_t = 3.22, \overline{Nu}_t = 5.47$, $N_B = 192, N_I = 983, 1455$

4.2 Case 2: Two heated steps on the top and bottom walls

Instead of heated parts, two heated steps are located at the top and bottom walls. The aspect ratio which is the ratio of the length of the obstacle to the cavity height is considered as $h_b = 1/5$.

In Fig. 4, the center of each streamline bundle expands giving stagnant regions symmetrically located on both parts of the cavity separated by obstacles. Thus, the fluid movement slows down when Da gets smaller due to the decrease in permeability of the porous medium. For large values of Da, temperature gradient clusters through left and right sides of bottom heated step with a similar formation through the left and right up corners of the cavity. This is an evidence of dominance of convection in the cavity for large values of Da. However, heat transfer is suppressed as the conductive heat transfer increases with the decrease in Darcy number. Vorticity becomes stagnant at the center forming boundary layers through the walls for small values of Da.

Figure 5 shows that the centered circulations in streamlines expand horizontally for large values of Ra, and boundary layers are formed for streamlines between symmetric cells as well as through the left and right walls. The expected behavior as natural convection is observed in isotherms when Ra is increased. Isotherms are forced to be parallel to adiabatic walls. Vorticity is not affected much with an increase in Ra. When the size of the step is decreased (Fig. 6), convective behavior of the fluid becomes more clear. All contours take a similar form as in Fig. 3 for $h_a = 1/7$.

Average Nusselt number changes in a similar way on the top and bottom obstacles as can be seen from Fig. 7 ($Ra = 10^6$). For small values of Darcy number ($Da \leq 10^{-4}$), heat transfer is suppressed, and the conductive heat transfer is pronounced for all values of porosity (average Nusselt number tends to be constant). The increase in convective heat transfer emerges with the increase in Darcy number due to the

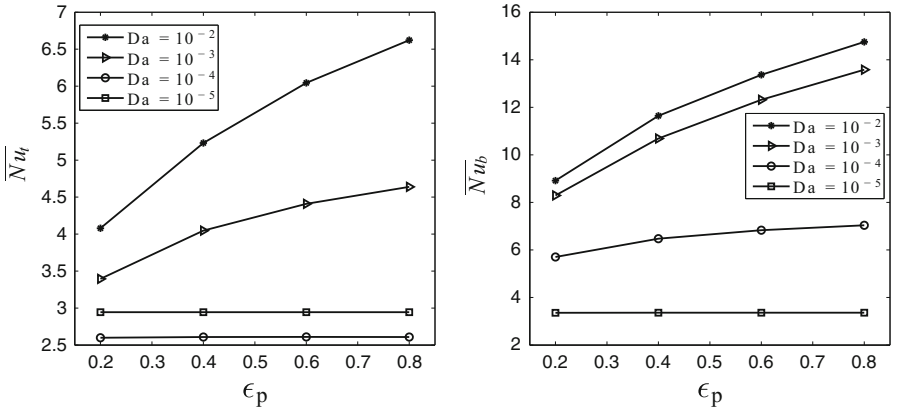

Fig. 7 Average Nusselt number variation through *top* and *bottom* obstacle walls

increasing permeability of the porous medium resulting with faster flow. Further, for a fixed Darcy number, the increase in average Nusselt number as porosity increases is observed. This is due to the fact that the dimensionless velocity increases while the inertial (Forchheimer) and non-linear drag ($\mathbf{u}.\nabla\mathbf{u}$) terms become less significant as porosity increases. Moreover, heat transfer at the bottom step is higher than the top step since the two symmetric, counter rotating cells are met at the bottom step for large values of Da. Therefore, the fluid circulation around the bottom step becomes much higher than the top step. In other words, much more heated flow circulates through the bottom step.

In both cases, the effects of Darcy number, Rayleigh number and the porosity of the porous medium on natural convection are in accordance with the natural convection flow behavior investigated in [12,16].

5 Conclusion

In this study, the Brinkman–Forchheimer-extended Darcy model is numerically investigated using DRBEM. DRBEM has the advantage of resulting in small sized algebraic systems due to its boundary only nature. Even though the two different geometries are studied, the main results are the same for both cases. The small values of Darcy number Da and porosity ϵ_p have a suppressing effect on the fluid flow and heat transfer, and the increase in Ra causes the heat transfer to be convective.

References

1. K. Al-Farhany, A. Turan, Non-Darcy effects on conjugate double-diffusive natural convection in a variable porous layer sandwiched by finite thickness walls. Int. J. Heat Mass Transf. **54**, 2868–2879 (2011)
2. C. Beckermann, S. Ramadhyani, R. Viskanta, Natural convection flow and heat transfer between a fluid layer and a porous layer inside a rectangular enclosure. Trans. ASME J. Heat Transf. **109**, 363–370 (1987)

3. M. Bhuvaneswari, S. Sivasankaran, Y.J. Kim, Effect of aspect ratio on convection in porous enclosure with partially active thermal walls. Comput. Math. Appl. **62**, 3844–3856 (2011)
4. X.B. Chen, P. Yu, S.H. Winoto, H.T. Low, Free convection in a porous wavy cavity based on the Darcy–Brinkman–Forchheimer extended model. Numer. Heat Transf. Part A **52**, 377–397 (2007)
5. S. Das, R.K. Sahoo, Effect of Darcy, fluid Rayleigh and heat generation parameters on natural convection in a porous square enclosure: a Brinkman-extended Darcy model. Int. Commun. Heat Mass Transf. **26**, 569–578 (1999)
6. R. Jecl, L. Skerget, Boundary element method for natural convection in non-Newtonian fluid saturated square porous cavity. Eng. Anal. Bound. Elem. **27**, 963–975 (2003)
7. M. Karimi-Fard, M.C. Charrier-Mojtabi, K. Vafai, Non-Darcian effects on double-diffusive convection within a porous medium. Numer. Heat Transf. Part A **31**, 837–852 (1997)
8. K.M. Khanafer, A.J. Chamkha, Mixed convection flow in a lid-driven enclosure filled with a fluid-saturated porous medium. Int. J. Heat Mass Transf. **42**, 2465–2481 (1999)
9. K. Khanafer, B. Al-Azmi, A. Marafie, I. Pop, Non-Darcian effects on natural convection heat transfer in a wavy porous enclosure. Int. J. Heat Mass Transf. **52**, 1887–1896 (2009)
10. S.A. Khashan, A.M. Al-Amiri, I. Pop, Numerical simulation of natural convection heat transfer in a porous cavity heated from below using a non-Darcian and thermal non-equilibrium model. Int. J. Heat Mass Transf. **49**, 1039–1049 (2006)
11. D.S. Kumar, A.K. Dass, A. Dewan, Analysis of Non-Darcy models for mixed convection in a porous cavity using a multigrid approach. Numer. Heat Transf. Part A **56**, 685–708 (2009)
12. P.A.K. Lam, K.A. Prakash, A numerical study on natural convection and entropy generation in a porous enclosure with heat sources. Int. J. Heat Mass Transf. **69**, 390–407 (2014)
13. H.Y. Li, K.C. Leong, L.W. Jin, J.C. Chai, Analysis of fluid flow and heat transfer in a channel with staggered porous blocks. Int. J. Therm. Sci **49**, 950–962 (2010)
14. A. Narasimhan, *Essentials of Heat and Fluid Flow in Porous Media* (CRC Press; Taylor & Francis Group, 2013)
15. D.A. Nield, A. Bejan, *Convection in Porous Media* (Springer, Berlin, 2006)
16. P. Nithiarasu, K.N. Seetharamu, T. Sundararajan, Natural convective heat transfer in a fluid saturated variable porosity medium. Int. J. Heat Mass Transf. **40**, 3955–3967 (1997)
17. P. Nithiarasu, K.N. Seetharamu, T. Sundararajan, Effect of porosity on natural convective heat transfer in a fluid saturated porous medium. Int. J. Heat Fluid Flow **19**, 56–58 (1998)
18. P. Nithiarasu, K.N. Seetharamu, T. Sundararajan, Finite element modelling of flow, heat and mass transfer in fluid saturated porous media. Arch. Comput. Methods Eng. **9**, 3–42 (2002)
19. W. Pakdee, P. Rattanadecho, Unsteady effects on natural convective heat transfer through porous media in cavity due to top surface partial convection. Int. J. Heat Mass Transf. **26**, 2316–2326 (2006)
20. P.W. Partridge, C.A. Brebbia, L.C. Wrobel, *The Dual Reciprocity Boundary Element Method* (Computational Mechanics Publications, Elsevier, Southampton, London, 1992)
21. B.V. Rathish Kumar, Shalini, Free convection in a non-Darcian wavy porous enclosure. Int. J. Eng. Sci **41**, 1827–1848 (2003)
22. H. Saleh, A.Y.N. Alhashash, I. Hashim, Rotation effects in an enclosure filled with porous medium. Int. Commun. Heat Mass Transf. **43**, 105–111 (2013)
23. B. Sarler, J. Perko, D. Gobin, B. Goyeau, H. Power, Dual reciprocity boundary element method solution of natural convection in Darcy–Brinkman porous media. Eng. Anal. Bound. Elem. **28**, 23–41 (2004)